Resonant production of sterile neutrinos in the early universe

Lauren Gilbert[1,*]

[1] *California Institute of Technology*

(Dated: May 13, 2016)

Abstract

We examine the cosmological impacts of a light resonantly produced sterile neutrino in the early universe. Such a neutrino could be produced through lepton number-driven Mikheyev-Smirnov-Wolfenstein conversion of active neutrinos, resulting in a non-thermal spectrum of both sterile and active neutrinos. If this process occurs during weak decoupling and big bang nucleosynthesis, it would affect the electron neutrino flux and therefore the n/p ratio. This allows us to use observations of primordial helium (Y_p), primordial deuterium (D/H), and N_{eff} to place limits on this process.

* lgilbert@caltech.edu

I. INTRODUCTION

Neutrinos are some of the least well understood particles in the Standard Model. They are nearly massless (≤ 2 eV) and interact only with the weak force and gravity. Given their lack of mass, and the low interaction cross-section of the weak force, they interact with other matter infrequently.

Neutrino mass eigenstates and flavor eigenstates (ν_e, ν_μ, ν_τ) are not coincident, but rather, related by a unitary transformation. Flavor states are weak interaction eigenstates, while the energy eigenstates are commonly referred to as mass eigenstates. For a two-state system, they are:

$$E_1 = \left(p^2 + m_1^2\right)^{1/2} \tag{1}$$

$$E_2 = \left(p^2 + m_2^2\right)^{1/2} \tag{2}$$

... where E is the energy, p is the three momentum, and m_1 and m_2 are the mass eigenstates.

The matrix used in the unitary transformation between the flavor and mass basis is known as the Pontecorvo-Maki-Nakagawa-Sakata (MNS) matrix, and is the neutrino analogue to the Cabibbo-Kobayashi-Maskawa (CKM) matrix. Since there are believed to be three flavors of neutrinos, the matrix can be parameterized into three angles and a CP violating phase. However, neither the absolute masses nor mass hierarchy ($\Delta m_{12} > \Delta m_{23}$ or $\Delta m_{12} < \Delta m_{23}$) have been experimentally determined. The CP violating phase is also unknown.

There are a number of controversial experimental hints that the current three-flavor neutrino model is not sufficient. Both MiniBooNE and LSND detected an excess of low-energy events that would indicate a higher rate of $\nu_\mu \rightarrow \nu_e$ appearance than expected [1]. Furthermore, several reactor-based experiments (Gosgen, SRP, ILL, Bugey, etc.) have seen fewer than expected antineutrino [2]. Gallium-based solar neutrino experiments (GALLEX and SAGE) have also seen several percent fewer antineutrino events than expected [3].

All of these suggest that there might be a fourth type of neutrino. All currently known neutrinos are left-handed; no right-handed neutrinos have ever detected, nor any left-handed antineutrinos. It is possible that right-handed neutrinos (and left-handed antineutrinos) are "sterile" – that is, they do not interact with the weak force. Such particles would be nearly undetectable, given the already-low interaction cross-section of active neutrinos.

While unlikely to interact directly, sterile neutrinos could affect the interactions of active neutrinos. As neutrinos oscillate from electron to mu to tau flavors, they could also oscillate to a sterile state.

We consider two neutrino flavor eigenstates. Any unitary transformation can be parameterized in terms of angles (though they have no geometric meaning). In this case, we can use a single angle:

$$|\nu_e\rangle = \cos\theta|\nu_1\rangle + \sin\theta|\nu_2\rangle \tag{3}$$

$$|\nu_s\rangle = -\sin\theta|\nu_1\rangle + \cos\theta|\nu_2\rangle \tag{4}$$

... where $|\nu_1\rangle$ and $|\nu_2\rangle$ are mass eigenstates, and θ is the vacuum mixing angle. A neutrino in a given mass state is therefore a superposition of active and sterile states, though assuming θ is small, the flavor and mass eigenstates are roughly coincident. We define:

$$\delta m^2 = m_2^2 - m_1^2 \tag{5}$$

The interaction cross-section of an active neutrino is:

$$\sigma_{\nu_e} \sim G_F^2 E^2 \tag{6}$$

... where G_F is the Fermi constant:

$$G_F = 1.166 * 10^{-5}\ \text{GeV}^{-2} \tag{7}$$

From eq. 4, the interaction cross-section of a sterile neutrino is:

$$\sigma_{\nu_s} \sim G_F^2 E^2 \sin^2\theta \tag{8}$$

Neutrino interactions impact the synthesis of nuclei, as freeze-out from nuclear statistical equilibrium determines light element abundances, and the neutron-to-proton ratio (n/p ratio) is an important parameter in this process. This parameter is affected by the competition between weak interactions that make neutrons and weak interactions that make neutrons. The abundances of light nuclei are set during big bang nucleosynthesis (BBN) at the temperature scale $\sim$ 1 MeV. The temperature scale is roughly coincident with weak decoupling and freeze-out.

At very high temperatures, neutrinos are in thermal and chemical equilibrium with the plasma (which consists of γ, $e^{\pm}$, neutrons, and protons). As the temperature of the universe

FIG. 1. Weak reaction rates vs. temperature, from [13].

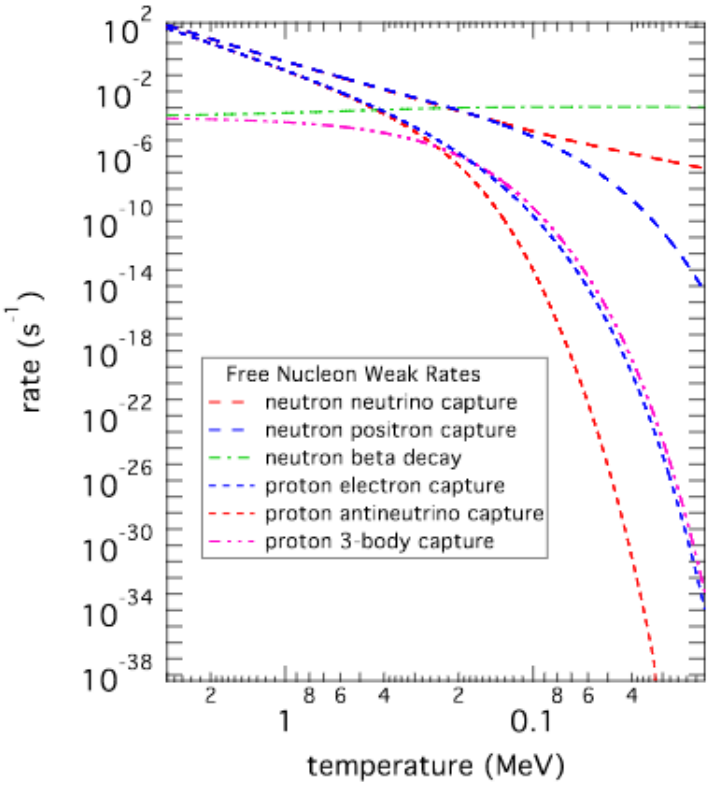

drops, the scattering rate of neutrinos drops below the expansion rate of the universe, and the neutrinos can no longer efficiently exchange energy with the plasma. This is called weak decoupling. This happens around ~ 1 MeV.

The rate of iso-spin flip (neutron to proton conversion and vice versa) is fast in comparison to the expansion rate of the universe at high temperature. As the temperature decreases, the weak interaction rates drop, as shown in fig. 1. Proton-to-neutron conversion drops off first, since it is energetically less favorable, while neutrons continue to be converted in protons via neutrino capture. The rate of iso-spin flip falls below the expansion rate of the universe and the neutron to proton ratio freezes out.

The forward and reverse reactions of proton-to-neutron conversions are:

$$\mathrm{n} + \mathrm{e}^+ \rightleftharpoons \bar{\nu}_\mathrm{e} + \mathrm{p} \tag{9}$$

$$\mathrm{n} + \nu_\mathrm{e} \rightleftharpoons \mathrm{p} + \mathrm{e}^- \tag{10}$$

$$n \rightleftharpoons p + e^- + \bar{\nu}_e \tag{11}$$

As the above reactions slow, the neutron-to-proton ratio freezes out – free neutron decay

continues. By ∼0.7 MeV, the n/p ratio is 1:6, but by the time alpha particles form, the ratio is approximately 1:7. Weak freeze-out and weak decoupling occur when the weak interaction rate ($\lambda_{weak} \sim G_F^2 T^5$) falls below the Hubble expansion rate ($\mathrm{H} = \sqrt{8\pi G\rho_c/3} \sim T^2/m_{Pl}$). However, unlike photon decoupling, weak freeze-out and decoupling are not instantaneous; rather, they take ∼ 10 Hubble times. For the purposes of this calculation, we assume sharp decoupling at a temperature 30 MeV.

In BBN, alpha particles assemble when the temperature drops to ≈ 0.1 MeV. The vast majority of the neutrons are incorporated into alpha particles, although about 1 in 10^5 neutrons are incorporated into deuterium nuclei. Very small amounts of tritium, lithium-7 and beryllium-7 are also produced during BBN.

If neutrinos oscillate between active and sterile flavors, the physics of sterile neutrinos impacts the electron neutrino flux. As seen in eq. 10, if we convert electron neutrinos into sterile neutrinos, that will reduce the rate of ν_e capture and the ratio of neutrons to protons will increase (compared to a scenario with no sterile neutrinos).

The predicted helium-4 and deuterium abundances in standard BBN (with no sterile neutrinos) have matched observation relatively well, though there are some hints of beyond Standard Model physics in the deuterium abundance [4]. The addition of a sterile neutrino – fully thermalized or not – could significantly change elemental abundances.

In the next 10 years, 30m class telescopes hope to measure the primordial deuterium abundance to within 3% from low-metallicity damped Lyman-α systems [5] . With this data, beyond Standard Model physics that affects deuterium production by 2% can be experimentally constrained in the near future.

In addition to elemental abundances, neutrino physics can be constrained from cosmic microwave background (CMB) physics. In the weak decoupling epoch, annihilating electron-positron pairs transfer their entropy to photons, not to neutrinos as they are decoupled. Therefore, the photon temperature is slightly higher than the neutrino temperature:

$$\frac{T_\gamma}{T_\nu} = \left(\frac{11}{4}\right)^{\frac{1}{3}} \tag{12}$$

From this, we can determine the relativistic energy density in terms of the photon energy density (measurable from the CMB):

$$\rho_r = \left[1 + \frac{7}{8}\left(\frac{4}{11}\right)^{\frac{1}{3}} N_{eff}\right] \rho_\gamma \tag{13}$$

... where N_{eff} is the effective number of degrees of freedom – the "effective number of neutrinos". $N_{eff} = 3$ would correspond to 3 fully thermalized species (flavors) of neutrinos and anti-neutrinos with Fermi-Dirac blackbody spectra. Finite temperature quantum electrodynamic corrections and Boltzmann energy transport during weak decoupling result in a theoretical N_{eff} value of 3.046 [6].

If sterile neutrinos were fully thermalized through their mixing with active neutrinos, then they would "count" as an extra neutrino species in N_{eff}. However, their mixing angles may not be large enough for them to thermalize and in that case, they could contribute fractional amounts to N_{eff}.

Current cosmological measurements do not rule out such neutrinos – Planck's 2015 results reported N_{eff} as $3.04^{+0.33}_{-0.34}$ and the sum of the light neutrino masses as <0.194 eV [7].

Particularly, we consider the lepton number-driven MSW-like transformation of active neutrinos to light sterile neutrinos in the epoch of the early universe during and after weak decoupling. We focus on sterile neutrinos with mass $\sim$ 1 eV - 10 eV, vacuum mixing angle $\sin 2\theta$ 10^{-2} - 10^{-4}, and lepton number $< 5 * 10^{-2}$. The reason for selecting these parameters will be discussed below. We assume no sterile neutrinos are produced prior to weak decoupling.

Resonant production of somewhat higher mass sterile neutrinos ($\sim$ keV) may provide a candidate for warm or cold dark matter [8]. These neutrinos are beyond the scope of this paper, but may require a non-zero lepton number, as we discuss here.

II. METHODOLOGY

A. Theory

Adiabatic flavor transformation corresponds to the oscillation length at resonance being small in comparison to the resonance width. In vacuum, the sterile neutrino state corresponds to a much higher mass than an active neutrino state. However, as an active neutrino propagates through medium, it acquires an effective mass. When the effective mass of an active state is roughly the mass associated with the sterile state, that is called a mass level crossing. That, in turn, corresponds to a MSW resonance.

We determine the transition probability in terms of the resonance width and the oscil-

lation length at resonance. The resonance width, δt, is defined in terms of the forward scattering potential for an active neutrino.

$$\delta t = \left(\frac{1}{V}\frac{dV}{dt}\right)^{-1} \tan 2\theta \tag{14}$$

The potential (V) is discussed in more detail below. The potential scale height, that is, the time scale over which the potential changes appreciably, is:

$$D = \left(\frac{1}{V}\frac{dV}{dt}\right)^{-1} \tag{15}$$

The Hubble parameter is defined as:

$$H = \sqrt{\frac{8\pi G\rho}{3}} \tag{16}$$

In radiation-dominated conditions, $\rho \sim T^4$ so:

$$H \sim \frac{T^2}{m_{Pl}} \tag{17}$$

... where m_{Pl} is the Planck mass. Very roughly, the potential scale height is H^{-1}, implying that:

$$\delta t \sim H^{-1} \tan 2\theta \tag{18}$$

For fixed vacuum mixing angle and fixed vacuum mass squared difference, the oscillation length is the distance traveled where the probability of finding a neutrino initially in state α again in state α is 1 as shown as in fig. 2. The oscillation length at resonance is different than the oscillation length in vacuum. This is because the effective masses and effective mixing angle change in medium, and the effective mass squared difference is at a minimum at an MSW resonance. The oscillation length at an MSW resonance is:

$$L_{osc}^{res} = \frac{4\pi E_\nu}{\delta m^2 \sin 2\theta} \tag{19}$$

The Landau-Zener jump probability, as derived in [9], is:

$$P_{LZ} = e^{-\pi\gamma/2} \tag{20}$$

In this expression, the adiabaticity parameter, proportional to the ratio of the resonance width to the oscillation length at resonance is:

$$\gamma = \frac{2\pi\delta t}{(\hbar c) L_{osc}^{res}} = \frac{1}{2}\left(\frac{1}{V}\frac{dV}{dt}\right)^{-1} \frac{\delta m^2}{(\hbar c) E_\nu} \frac{\sin^2 2\theta}{\cos 2\theta} \tag{21}$$

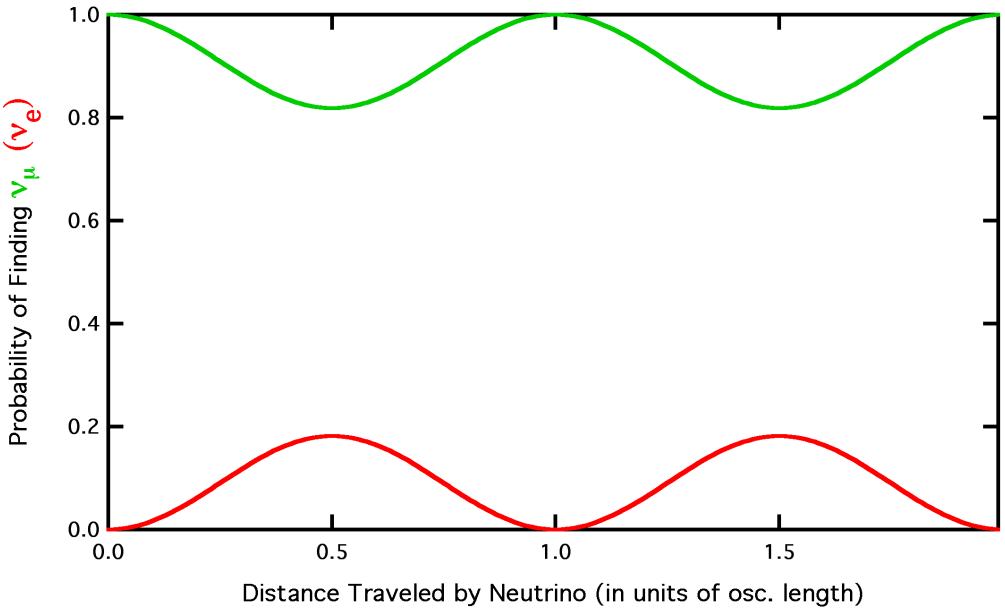

FIG. 2. The oscillation length is the distance traveled by a neutrino ν_α where the probability of returning to state ν_α is 1.

The probability that an electron propagates through the resonance region and becomes a sterile neutrino is:

$$P_{\nu_e \to \nu_s} = 1 - P_{LZ} = 1 - e^{-\pi\gamma/2} \tag{22}$$

Note that complete conversion corresponds to large values of the adiabaticity parameter. This, in turn, corresponds to oscillation lengths at resonance that are small compared to the resonance width. From this, it is easy to see that the larger the mixing angle, the likelier such a conversion will be. Likewise, the lower the energy, the more likely conversion will be. Finally, note that the larger δm^2, i.e. the larger the sterile neutrino mass, the adiabatic sterile neutrino conversion will be.

There are two components to the potential from forward scattering: the "density" term and the "thermal "term. We consider the thermal term first. Electron neutrinos can forward-scatter on $e^{\pm}$ and a virtual Z boson. This potential is defined in terms of the number densities of electrons and positrons (n_{e^-}, n_{e^+}), Fermi constant (G_F), Z boson mass (m_Z) and average energy of electrons/positions ($\langle E_{e^-}\rangle$, $\langle E_{e^+}\rangle$).

$$V_{T,\nu_e} = -\frac{8\sqrt{2}G_F}{3m_Z^2}\left[\langle E_{e^-}\rangle n_{e^-} + \langle E_{e^+}\rangle n_{e^+}\right] \tag{23}$$

A neutrino of any flavor sees a charged current forward scattering potential with a vir-

tual W boson and a neutrino of the same flavor. This is defined in terms of the number density of that neutrino flavor neutrino (n_{ν_α}, $n_{\bar{\nu}_\alpha}$), Fermi constant (G_F), average energy of neutrinos/anti-neutrinos ($\langle E_{\nu_\alpha}\rangle$, $\langle E_{\bar{\nu}_\alpha}\rangle$) and W boson mass ($m_W$).

$$V_{T,\nu_\alpha} = -\frac{8\sqrt{2}G_F}{3m_W^2}\left[\langle E_{\nu_\alpha}\rangle n_{\nu_\alpha} + \langle E_{\bar{\nu}_\alpha}\rangle n_{\bar{\nu}_\alpha}\right] \tag{24}$$

We can write both potentials in a form parameterized in terms of a constant r_α that is determined by the flavor state.

$$V = -r_\alpha G_F^2 \epsilon T^5 \tag{25}$$

We then consider the density term. We first define the Hamiltonians seen by active and sterile neutrinos. These will be defined in terms of the number densities of neutrinos (n_{ν_α}), Fermi constant (G_F), the number density of baryons (n_b) and electron fraction (Y_e, further defined below). The Hamiltonian seen by a sterile neutrino, even in matter, is simply zero, since it does not interact weakly.

$$H(\nu_s) = 0 \tag{26}$$

The "density" Hamiltonian for active neutrinos is somewhat more complex:

$$H(\nu_e) = V_D \frac{3\sqrt{2}}{2} G_F n_b \left(Y_e - \frac{1}{3}\right) + \sqrt{2}G_F\left(2\left(n_{\nu_e} - n_{\bar{\nu}_e}\right) + \left(n_{\nu_\mu} - n_{\bar{\nu}_\mu}\right) + \left(n_{\nu_\tau} - n_{\bar{\nu}_\tau}\right)\right) \tag{27}$$

During the relevant time period, the baryon-to-photon ratio is measured in the CMB to be:

$$\eta = \frac{n_b}{n_\gamma} \approx 6 * 10^{-10} \tag{28}$$

... where n_γ is the photon number density and is defined in terms of the Riemann zeta function:

$$n_\gamma = \frac{2\zeta(3)}{\pi^2} T^3 \tag{29}$$

$$\zeta(3) \approx 1.202 \tag{30}$$

... and n_b is baryon number. At temperatures large in comparison to the mass difference between neutrons and protons,

$$Y_e \approx \frac{1}{2} \tag{31}$$

However, we evolve the electron fraction throughout the BBN epoch with our code.

$$Y_e = \frac{n_e^- + n_e^+}{n_b} \tag{32}$$

... where n_{e^-}, n_{e^+}, and n_p are the number densities of electrons and positrons respectively.

We define:

$$\mathcal{L}_e = \frac{2\left(n_{\nu_e} - n_{\bar{\nu}_e}\right) + \left(n_{\nu_\mu} - n_{\bar{\nu}_\mu}\right) + \left(n_{\nu_\tau} - n_{\bar{\nu}_\tau}\right)}{n_\gamma} = 2L_e + L_\mu + L_\tau \tag{33}$$

This describes flavor asymmetries in the active neutrinos. We define lepton numbers L_{ν_α} as:

$$L_{\nu_\alpha} = \frac{n_{\nu_\alpha} - n_{\bar{\nu}_\alpha}}{n_\gamma} \tag{34}$$

Previous studies have determined that -0.01 $< L_{\nu_\alpha} <$ 0.07 [10]. (A negative lepton number would flip the behavior described to electron anti-neutrinos instead of electron neutrinos.) The lepton number is, in turn, defined in terms of chemical potential; this relationship is described in more detail in appendix A.

In terms of $\mathcal{L}_e$ write:

$$H(\nu_e) = V_D = \frac{2\sqrt{2}\zeta(3)G_F T^3}{\pi^2}\left(\mathcal{L}_e + \frac{3}{2}\eta\left(Y_e - \frac{1}{3}\right)\right) \tag{35}$$

The total potential is:

$$V = V_D + V_{T,\nu_\alpha} + V_{T,\nu_e} = \frac{2\sqrt{2}\zeta(3)G_F T^3}{\pi^2}\left(\mathcal{L}_e + \frac{3}{2}\left(Y_e - \frac{1}{3}\right)\eta\right) - r_\alpha G_F^2 \epsilon T^5 \tag{36}$$

As noted previously, when an active neutrino propagates through medium, it acquires an effective mass. When that mass is approximately the same as the sterile neutrino mass mass, an MSW resonance occurs. The MSW resonance condition is:

$$V = \frac{\delta m^2 \cos 2\theta}{2E_\nu} \tag{37}$$

This can be rewritten as:

$$\delta m^2 \cos 2\theta = 2\epsilon T V \tag{38}$$

... where:

$$\epsilon_{res} = E_\nu / T \tag{39}$$

The MSW resonance condition can be rewritten as:

$$\frac{4\sqrt{2}\zeta(3)G_F T^4 \epsilon_{res}}{\pi^2}\left(\mathcal{L}_e + \frac{3\eta Y_e}{2} - \frac{\eta}{2}\right) - 2r_\alpha G_F^2 \epsilon_{res}^2 T^6 = \delta m^2 \tag{40}$$

In this case, δm^2 is approximately the sterile neutrino mass squared. This results in a quadratic equation for ϵ_{res}. A solution is only possible when the following condition is met:

$$\frac{4(\zeta(3))^2 G_F}{\pi^2 \delta m^2 r_\alpha T^2}\left(\mathcal{L}_e + \frac{3}{2}\left(Y_e - \frac{1}{3}\right)\eta\right) \geq 1 \tag{41}$$

B. Implementation

We use the BURST code, which is more fully described in [11]. This uses the Kawano code for the nuclear reaction network ([12]) and a binned energy spectrum to follow the occupational probabilities through the BBN epoch. When the resonance condition is met, all electron neutrinos in a given energy bin are converted into sterile neutrinos.

In the early universe, the thermal term is relatively small, so we take r_α as zero, simplifying the potential from eq. 36 to:

$$V = \frac{2\sqrt{2}\zeta(3)G_F T^3}{\pi^2}\left(\mathcal{L}_e + \frac{3}{2}\left(Y_e - \frac{1}{3}\right)\eta\right) = \frac{\delta m^2 \cos 2\theta}{2E_\nu} \tag{42}$$

In this case, the resonance condition is:

$$\epsilon_{res} = \left(\frac{4\sqrt{2}\zeta(3)G_F T^4}{\pi^2 \delta m^2}\left(\mathcal{L}_e + \frac{3}{2}\left(Y_e - \frac{1}{3}\right)\eta\right)\right)^{-1} \tag{43}$$

As the universe expands and the temperature drops, ϵ_{res} sweeps from zero to higher values, converting electron neutrinos into sterile neutrinos. This is shown in fig. 3. This behavior is accentuated as lepton number is destroyed.

FIG. 3. Distribution function of electron and sterile neutrinos, where the vertical line gives the position of ϵ_{res}, the scaled resonance energy.

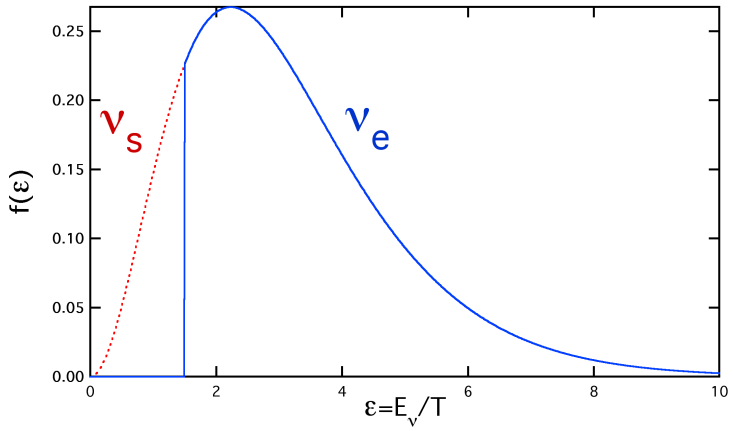

The initial spectrum of electron neutrinos is taken to be thermal, blackbody, Fermi-Dirac, and follows from:

$$f(\epsilon) = \frac{1}{\exp(\epsilon - \eta_{\nu_e}) + 1} \tag{44}$$

... where η_{ν_e} is μ_{ν_e}/T, where μ_{ν_e} is the chemical potential (see appendix A).

FIG. 4. Occupation probabilities of ν_e and ν_s with low ϵ_{res}.

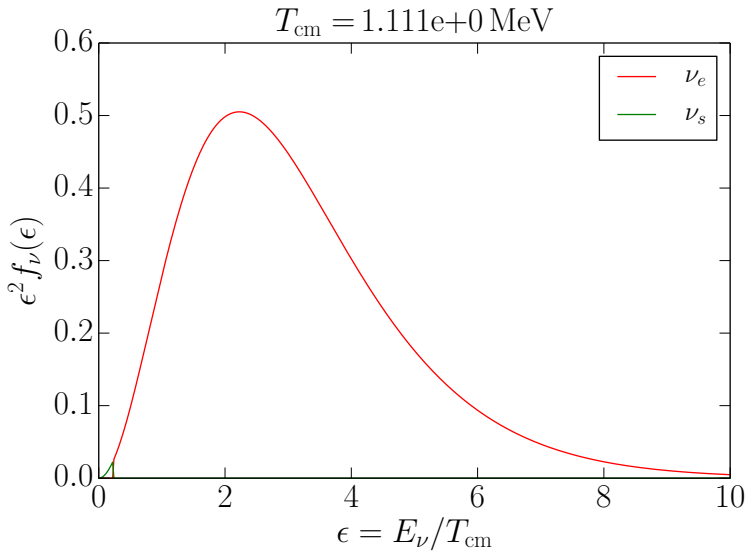

The occupational probabilities of electron neutrinos and sterile neutrinos are shown in figure 4. In this figure, a small number of bins have been converted into sterile neutrinos; the vertical line in the lower left corner corresponds to ϵ_{res}.

We follow the occupation probability through a range of scaled neutrino energy parameters $20 \geq \epsilon \geq 0$. The rate of this sweep increases as the lepton number is destroyed, which creates computational problems – ϵ_{res} does not proceed linearly with time. Since we have a binned energy spectrum, we must dynamically decrease the time step, to avoid skipping bins.

A spectrum after the sweep has completed is shown in fig. 5; the vertical line corresponds to ϵ_{res}, the energy under which sterile neutrino conversion occurs.

As we change the electron neutrino distribution function, we reduce the number of electron neutrinos and the neutron destruction rate. This will in turn result in a higher mass fraction of helium.

III. RESULTS

We plot the D/H mass fraction for a 1 eV sterile neutrino and $L_{e,\mu,\tau} = 10^{-2}$, 10^{-3}, and 10^{-4} in figure 6. When compared to measured D/H mass from [14], this shows clear tension. Adding some lepton number suppresses the production of deuterium, bringing our calculated values both with and without sterile neutrinos more in alignment with experimental values.

FIG. 5. Occupational probabilities of ν_e and ν_s at comoving temperature of 700 keV

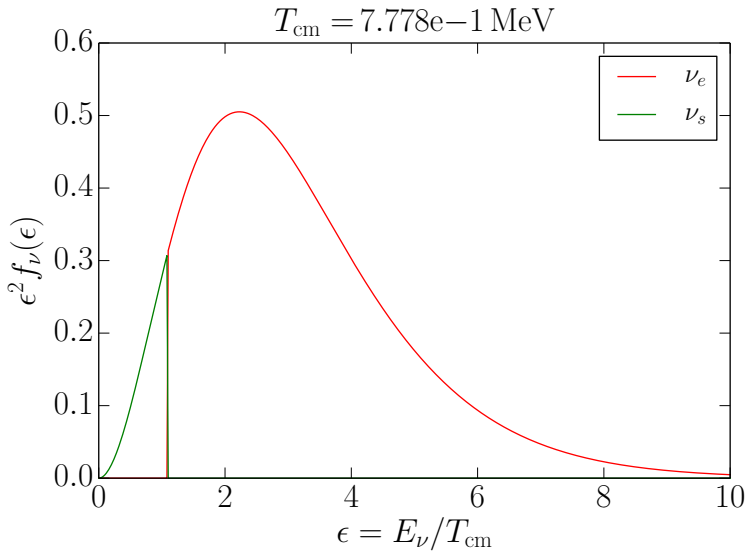

We also plot the ^{4}He mass fraction, again for a 1 eV sterile neutrino and $L_{e,\mu,\tau} = 10^{-2}$, 10^{-3}, and 10^{-4} in figure 7. We compare to Planck's measurement of $Y_p = 0.249^{+0.025}_{-0.026}$ [7] and Izotov, Thaun, and Guseva's measurement of $Y_p = 0.2465 \pm 0.0097$ [15].

We repeat the calculations for a 10 eV sterile neutrino in figs. 8 and 9. With a very large mixing angle ($3 * 10^{-1}$, $3 * 10^{-2}$) and large lepton number ($1 * 10^{-2}$), the results are unphysically large helium and deuterium fractions. However, smaller mixing angles and lepton numbers show physically reasonable behavior and are consistent with previous studies of light sterile neutrinos in the early universe [16].

We see that, for a given mass squared difference, as we increase the lepton number, the deuterium mass fraction increases and the helium mass fraction decreases. For a given lepton number and mass squared difference, an increase in mixing angle causes the helium and D/H mass fraction to increase.

A. Known issues

1. Deuterium and helium

We continue to have trouble with a binned energy spectrum; for large mixing angles and lepton numbers, ϵ_{res} jumps $\gg$ one bin at a time. While we recalculate for a smaller time step when this happens, it appears we do not do so to a sufficient degree; the resonance

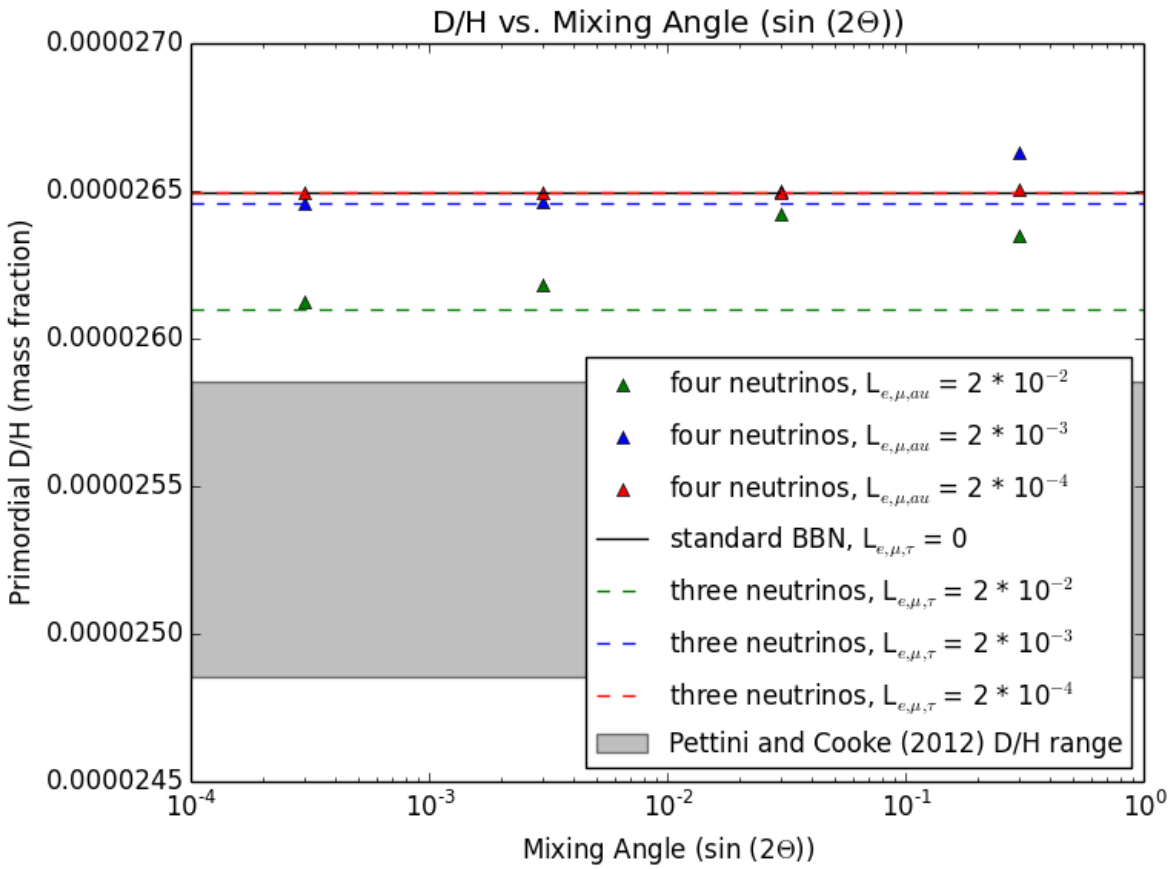

FIG. 6. Mass fraction of deuterium vs. sterile mixing angle, for a 1 eV sterile neutrino

simply changes too fast to be captured by our current code

For 10 eV sterile neutrinos with large mixing angles, the resonance simply skips to a bin past 1000, and while it continues to calculate a D/H and He yield, these are not correct. To fix this, we need to implement more (and smaller) time steps.

2. N_{eff}

As discussed in eq. 13, N_{eff} is a parametrization of the radiation energy density, and as such varies with the neutrino physics. As described in [17], N_{eff} is not identical to the CMB observable. The Planck observable, $\tilde{N}_{eff}$, is the ratio between the sound horizon and diffusion length. This reduces to N_{eff} for massless decoupled neutrinos. When we calculate $\tilde{N}_{eff}$ from these beyond Standard Model scenarios, it is clear that current constraints do not allow us to rule out any of these models, as shown in fig. 10.

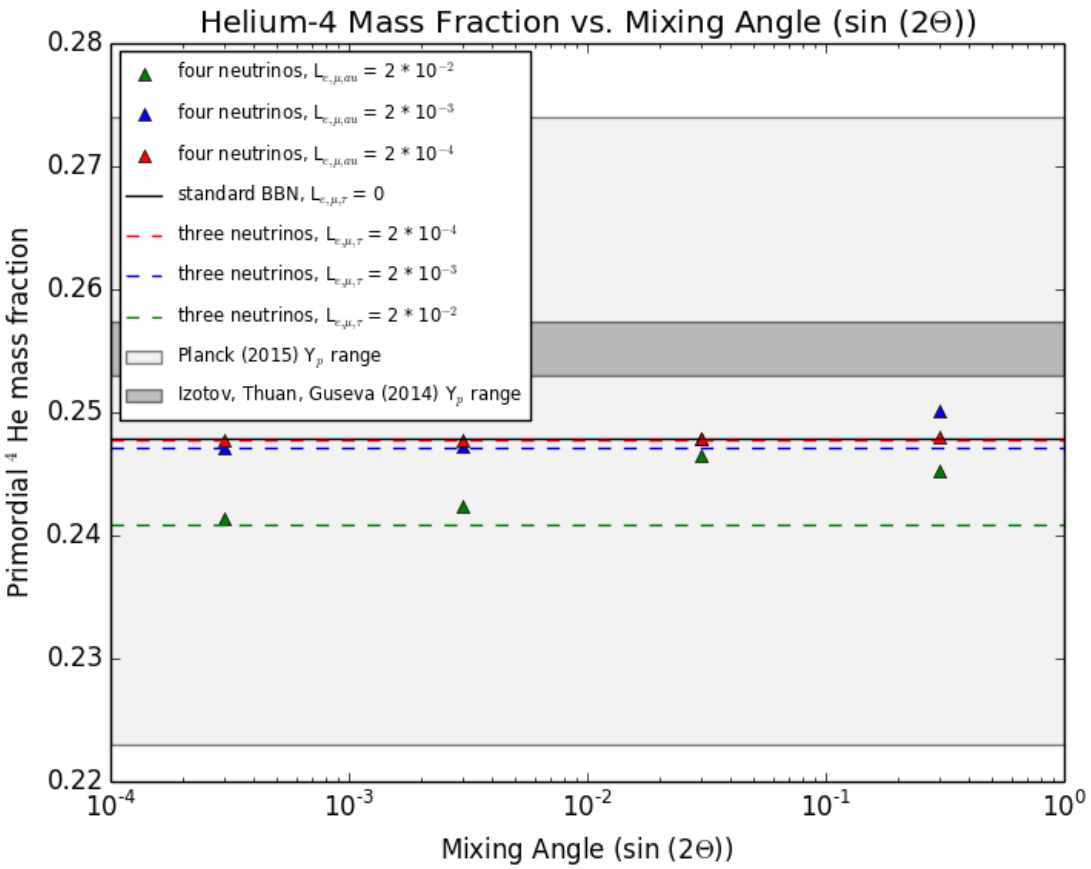

FIG. 7. Mass fraction of helium-4 vs. sterile mixing angle, for a 1 eV sterile neutrino

While Planck's constraints are insufficient to constrain the parameter space of a non-thermal sterile neutrino, fourth generation CMB experiments expect to contain N_{eff} to within 0.02, and $\sum m_\nu$ to within 0.15 meV. As shown in fig. 11, this may be sufficient to constrain models with non-thermal sterile neutrinos, albeit only ones with large masses and/or lepton numbers.

We also note that the behavior of N_{eff} with lepton number and mixing angle does not seem consistent; while the smaller mixing angles and lepton numbers behave as expected, the larger do not. Further work needs to be done to determine if these larger mixing angle/lepton number scenarios are accurate, and if so, if they will be constrainable from fourth generation CMB experiments.

The code is very much still a work in progress; we intend to continue refining the resonance sweep algorithm this summer until satisfied that it simulates physical reality.

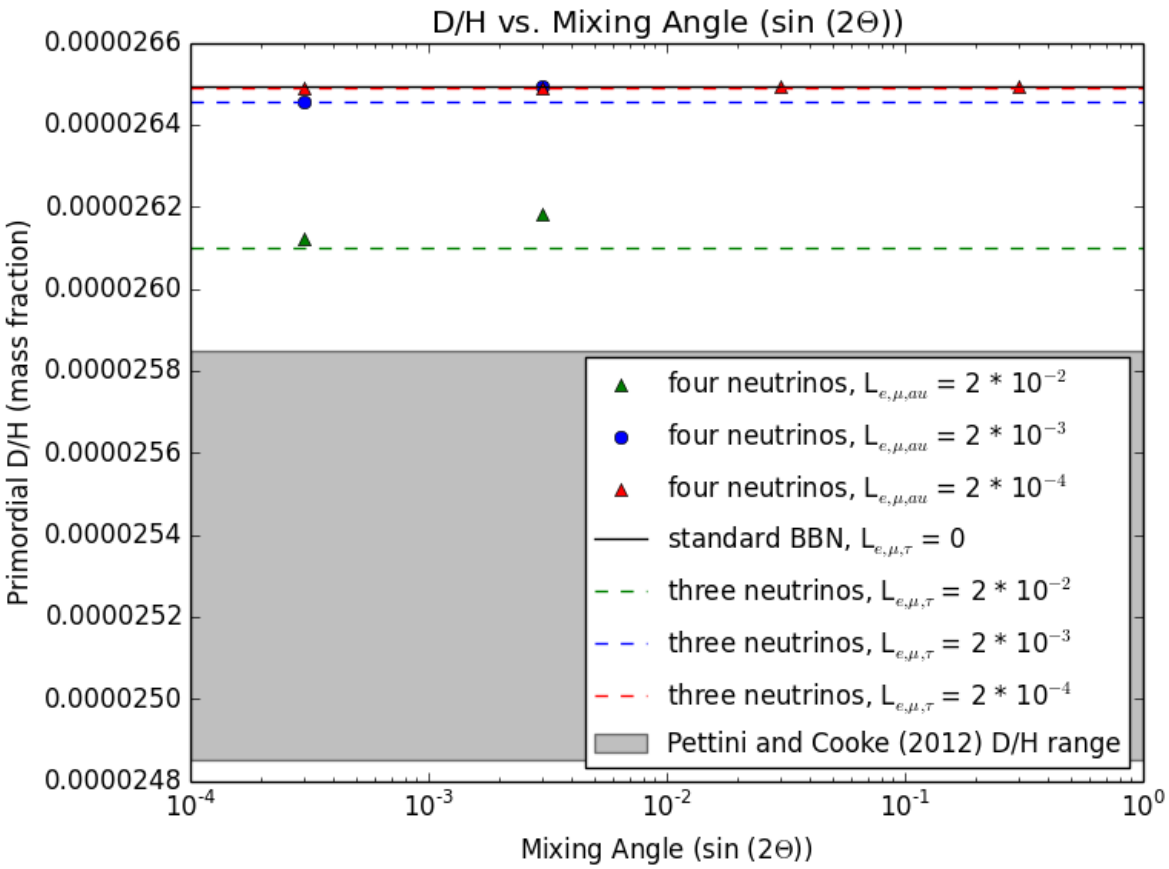

FIG. 8. Mass fraction of deuterium vs. sterile mixing angle, for a 10 eV sterile neutrino

IV. CONCLUSIONS

Active-sterile mixing can affect nuclear interaction rates and primordial elemental abundances. New, more precise measurements of D/H and helium will allow us to probe neutrino physics regimes not accessible by laboratory experiments for beyond Standard Model interactions. If observational limits on D/H and helium are reduced to ∼1%, we have some leverage to constrain sterile neutrino parameters.

Our study has revealed that this is a computational difficult problem; higher lepton numbers and smaller mixing angles will require further investigation.

V. ACKNOWLEDGEMENTS

LG extends profuse thanks to Evan Grohs (University of Michigan) and George Fuller (UCSD) for invaluable help. This research used resources provided by the Los Alamos

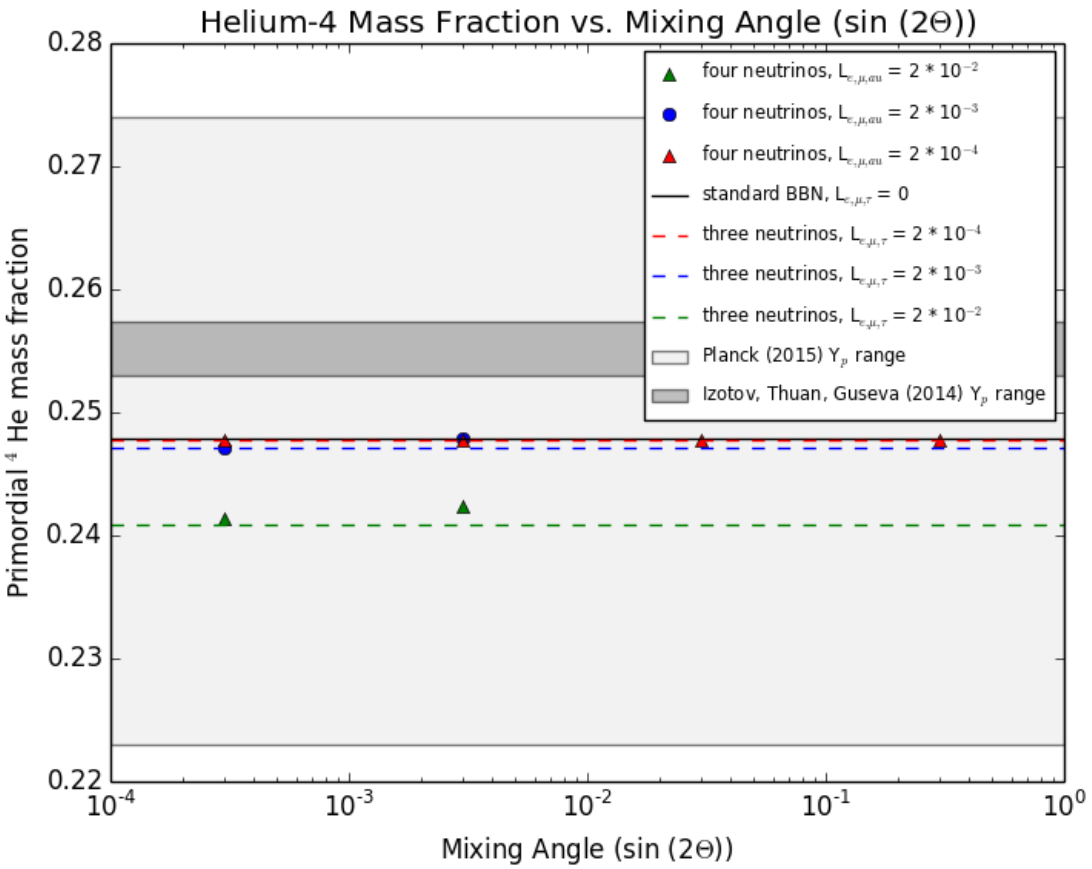

FIG. 9. Mass fraction of helium-4 vs. sterile mixing angle, for a 10 eV sterile neutrino

National Laboratory Institutional Computing Program, which is supported by the U.S. Department of Energy National Nuclear Security Administration under Contract No. DE-AC52-06NA25396.

Appendix A: Fermi Integrals, Distribution Functions, and Lepton Number

1. Relationship between chemical potential and distribution function

We consider a Fermi integral – that is, the integral that results from integration of a Fermi-Dirac distribution function for a particle with $\eta = \mu/\mathrm{T}$ (where μ is the chemical potential and T is temperature; note that this is not the same η as in equ. 28).

$$P(k) = \frac{x^k}{e^{x-\eta} + 1} \tag{A1}$$

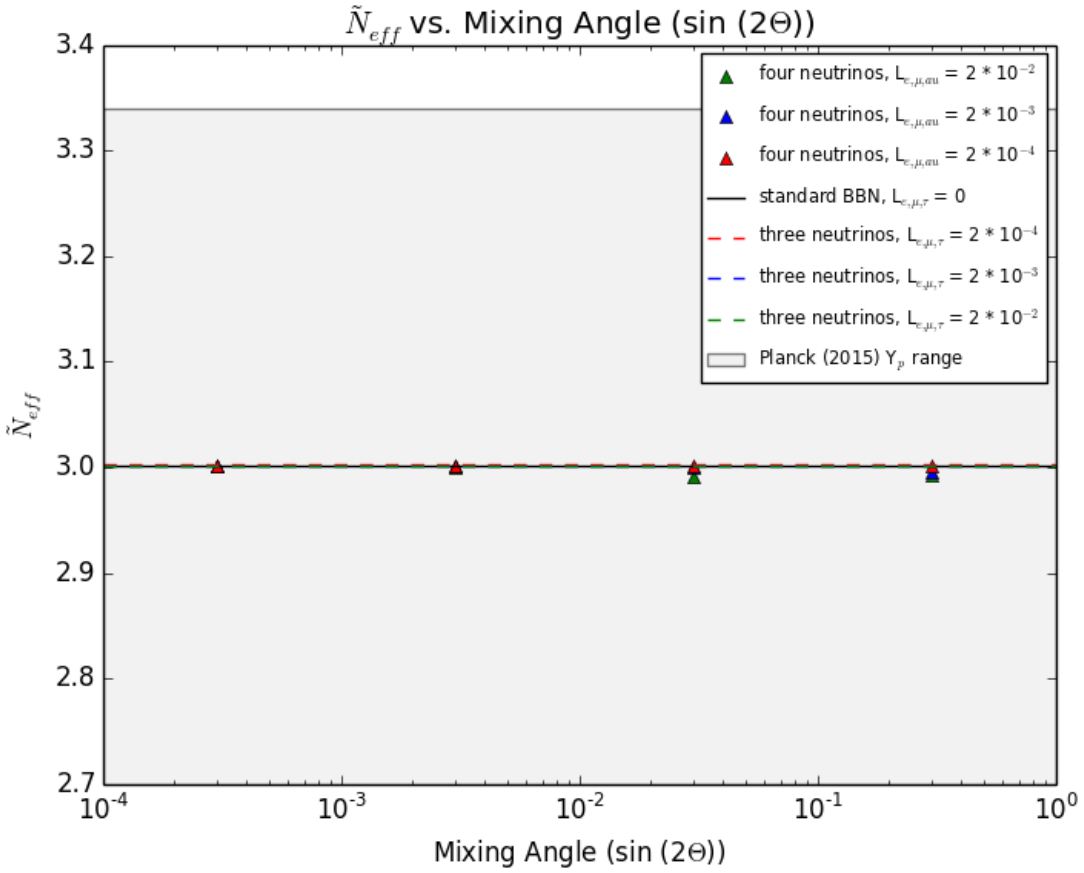

FIG. 10. $\tilde{N}_{eff}$ vs. sterile neutrino mixing angle, for a 1 eV sterile neutrino

$$F_k(\eta) = \int_0^\infty \frac{x^k dx}{e^{x-\eta}+1} \tag{A2}$$

$$\frac{dF_k}{d\eta} = \int_0^\infty \frac{x^k dx e^{x-\eta}}{(e^{x-\eta}+1)^2} = -\int_0^\infty \frac{-e^{x-\nu} dx x^k}{(e^{x-\eta}+1)^2} = -\frac{x^k}{e^{x-\eta}+1}\Big|_0^\infty + k\int_0^\infty \frac{x^{k-1}dx}{e^{x-\eta}+1} \tag{A3}$$

$$\frac{dF_k(\eta)}{d\eta} = kF_{k-1}(\eta) \tag{A4}$$

This provides a useful recursion relation.

$$dF_k(\eta) = kF_{k-1}(\eta)d\eta \tag{A5}$$

$$F_k(\eta) - F_k(0) = k\int_0^\infty F_{k-1}(\eta')d\eta' \tag{A6}$$

We consider the k = 0 case, as it is solvable analytically:

$$F_0(\eta) = \int_0^\infty \frac{dx}{e^{x-\eta}+1} = \int_0^\infty \frac{e^{\eta-x}dx}{1+e^{\eta-x}} \tag{A7}$$

$$u = 1 + e^{\eta-n} \tag{A8}$$

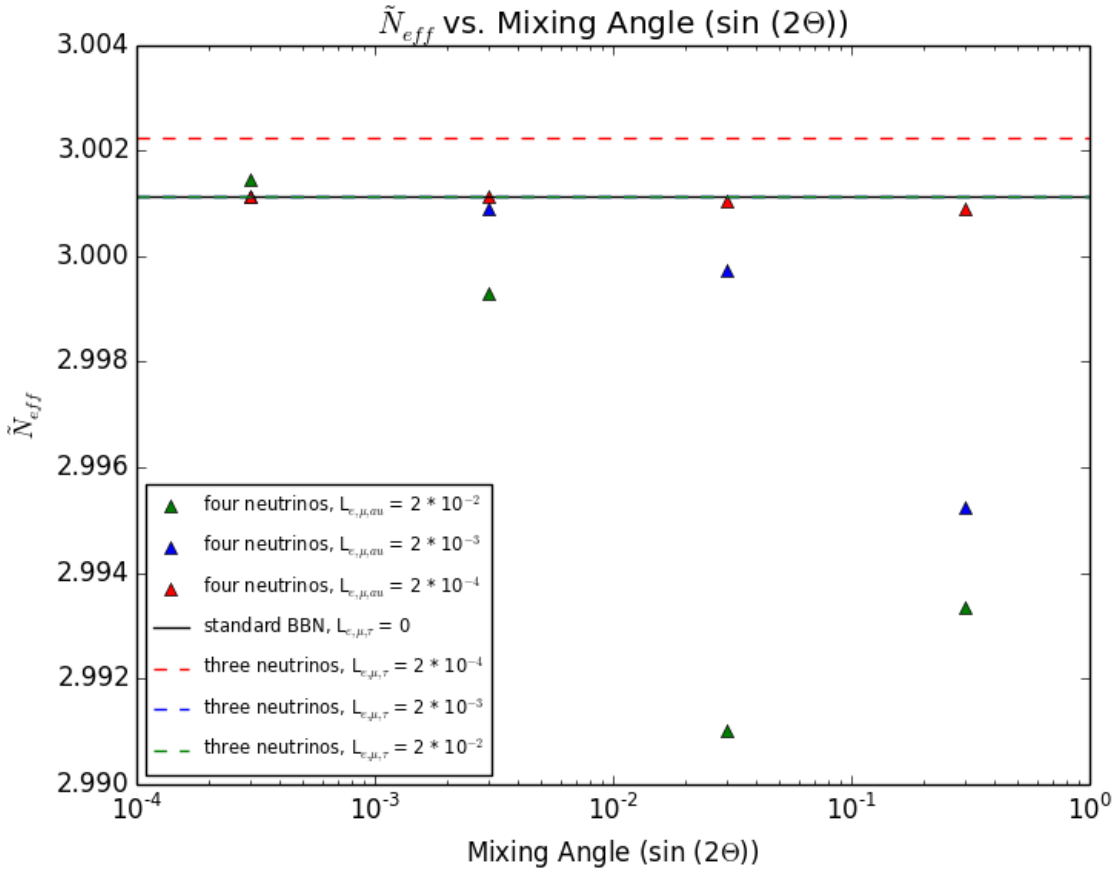

FIG. 11. $\tilde{N}_{eff}$ vs. sterile neutrino mixing angle, for 1 eV sterile neutrino

$$du = -e^{\eta - x} dx \tag{A9}$$

$$F_0(\eta) = -\int_{1+e^{\eta}}^{1} \frac{du}{u} = \ln(1 + e^{\eta}) = \ln[e^{\eta}(1 + e^{-\eta})] = \eta + \ln(1 + e^{-\eta}) \tag{A10}$$

$$F_0(-\eta) = \ln(1 + e^{-\eta}) \tag{A11}$$

$$F_0(\eta) - F_0(-\eta) = \eta \tag{A12}$$

We can integrate this to get:

$$\int_0^{\eta} F_0(\eta')d\eta' - \int_0^{\eta} F_0(-\eta')d\eta' = \int_0^{\eta} \eta' d\eta' = \frac{1}{2}\eta^2 \tag{A13}$$

We can apply eq. A6 to the above:

$$F_1(\eta) - F_1(0) + F_1(-\eta) - F_1(0) = \frac{1}{2}\eta^2 \tag{A14}$$

$$F_1(\eta) - F_1(-\eta) = \frac{1}{2}\eta^2 + 2F_1(0) \tag{A15}$$

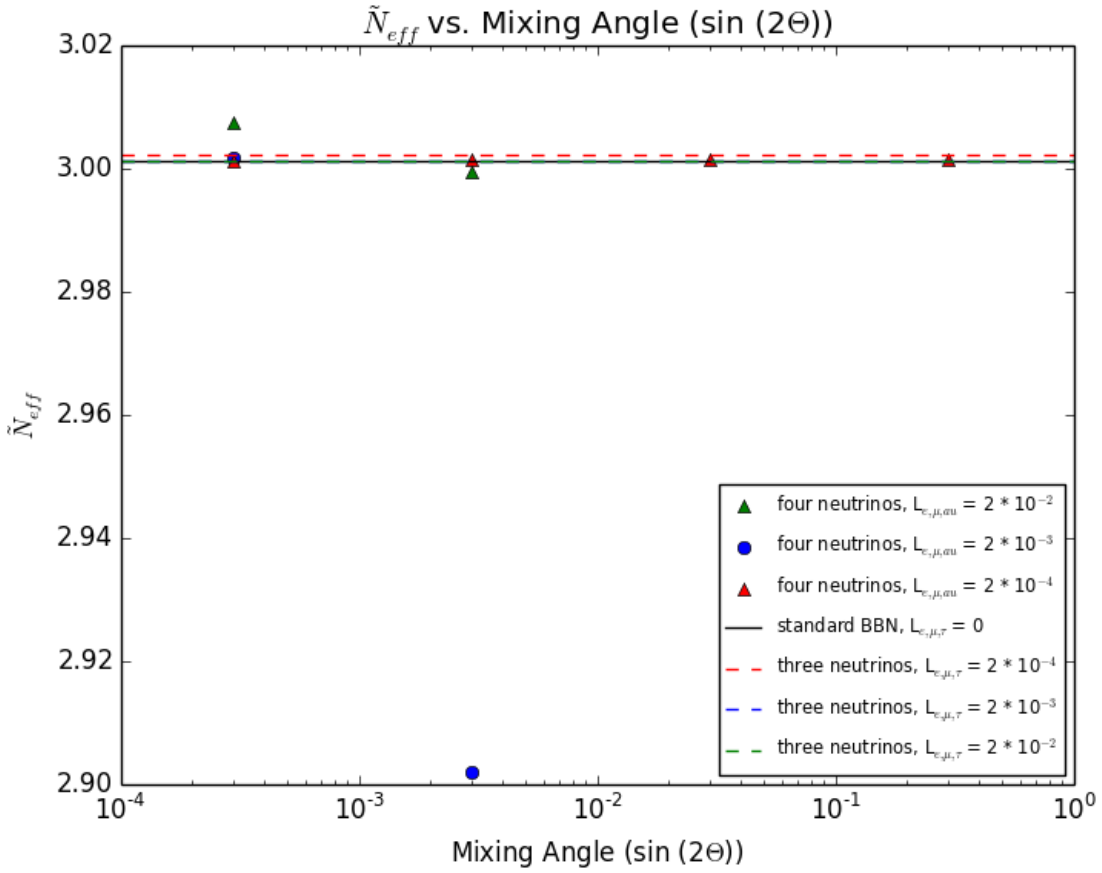

FIG. 12. $\tilde{N}_{eff}$ vs. sterile neutrino mixing angle, for 10 eV sterile neutrino

We apply eq. A6 again:

$$2\int_0^\eta F_1(\eta')d\eta' + 2\int_0^\eta F_1(-\eta')d\eta' = \frac{1}{3}\eta^3 + 4F_1(0)\eta \tag{A16}$$

$$F_2(\eta) - F_2(0) - (F_2(-\eta) - F_2(0)) = \frac{1}{3}\eta^3 + 4F_1(0)\eta \tag{A17}$$

$$F_2(\eta) - F_2(-\eta) = \frac{1}{3}\eta^3 + 4F_1(0)\eta \tag{A18}$$

Again applying A6,

$$3\int_0^\eta F_2(\eta')d\eta' - 3\int_0^\eta F_2(-\eta')d\eta' = \frac{1}{4}\eta^4 + 6F_1(0)\eta^2 \tag{A19}$$

$$F_3(\eta) - F_3(0) + F_3(-\eta) - F_3(0) = \frac{1}{4}\eta^4 + 6F_1(0)\eta^2 \tag{A20}$$

$$F_3(\eta) + F_3(-\eta) = \frac{1}{4}\eta^4 + 6F_1(0)\eta^2 + 2F_3(0) \tag{A21}$$

We now have several relationships between Fermi integrals and the chemical potential.

2. Neutrino number and energy density

In a classical case, with some number of particles in a 1D cavity of length l,

$$\lambda = \frac{ldk}{\pi} \tag{A22}$$

In a 3D cavity,

$$dN = \frac{l^3 d^3 k}{2\pi} \tag{A23}$$

However, we consider a quantum mechanical case, so this must be weighted by the Fermi-Dirac distribution function.

$$dn_\nu = g\frac{dk}{(2\pi)^3}\frac{1}{e^{E_\nu/T-\eta}+1} \tag{A24}$$

We note that in natural units ($\hbar = \mathrm{c} = 1$)

$$k = p \tag{A25}$$

and we write the differential as:

$$d^3k = d^3p = p^2 dp d\Omega \tag{A26}$$

and therefore the distribution function as:

$$n_{\nu_\alpha} = \frac{1}{(2\pi)^3}\int \frac{p^2 dp d\Omega}{e^{E_\nu/T-\eta}+1} \tag{A27}$$

Assuming no angular dependence:

$$n_{\nu_\alpha} = \frac{1}{2\pi^2}\int_0^\infty \frac{p^2 dp}{e^{E_\nu/T-\eta}+1} \tag{A28}$$

We find the energy:

$$E_\nu = (p_\nu^2 + m_\nu^2)^{1/2} \tag{A29}$$

$$dE_\nu = \frac{1}{2}(p_\nu^2 + m_\nu^2)^{-1/2} 2p_\nu dp = \frac{p_\nu dp_\nu}{E_\nu} \tag{A30}$$

$$E_\nu dE_\nu = pdp \tag{A31}$$

$$n_{\nu_\alpha} = \int_{m_\nu}^\infty \frac{pE_\nu dE_\nu}{e^{E_\nu/T-\eta}+1} \tag{A32}$$

Approximating m_ν as zero, we can write this:

$$n_{\nu_\alpha} = \frac{T_\nu}{2\pi^2}F_2(\eta) \tag{A33}$$

The number density for anti-neutrinos will depend on their chemical potential. We can prove this is simply $-\eta$:

$$\nu_\alpha + \nu_{\bar{\alpha}} \rightarrow 2\gamma \tag{A34}$$

$$\mu_{\nu_\alpha} + \mu_{\bar{\nu}_\alpha} = 0 \tag{A35}$$

$$\mu_{\nu_\alpha} = -\mu_{\bar{\nu}_\alpha} \tag{A36}$$

$$\eta_{\nu_\alpha} = -\eta_{\bar{\nu}_\alpha} \tag{A37}$$

$$n_{\bar{\nu}_\alpha} = \frac{T_\nu}{2\pi^2} F_2(-\eta) \tag{A38}$$

3. Lepton number

We define lepton number for a specific neutrino species as:

$$L_{\nu_\alpha} = \frac{n_{\nu_\alpha} - n_{\bar{\nu}_\alpha}}{n_\gamma} \tag{A39}$$

As derived in [18] for a particle obeying Bose-Einstein statistics,

$$n_\gamma = \frac{3\zeta(3)}{\pi^2} T_\gamma^3 \tag{A40}$$

$$L_{\nu_\alpha} = \frac{\pi^2}{2\zeta(3)} \frac{1}{T_\gamma^3} \left(\frac{T_\nu^3}{2\pi^2} \left(F_2(\eta_{\nu_\alpha}) - F_2(-\eta_{\nu_\alpha}) \right) \right) = \frac{1}{4\zeta(3)} \left(\frac{T_\nu}{T_\gamma} \right)^3 \left[\frac{1}{3} \eta_{\nu_\alpha} + 4F_1(0)\eta_{\nu_\alpha} \right] \tag{A41}$$

$$F_1(0) = \frac{\pi^2}{12} \tag{A42}$$

$$L_{\nu_\alpha} = \frac{\pi^2}{12\zeta(3)} \left(\frac{T_\nu}{T_\gamma} \right)^3 \left[n_{\nu_\alpha} + \frac{1}{\pi^2} \eta_{\nu_\alpha}^3 \right] \tag{A43}$$

Note that while eq. 12 holds at photon decoupling, it does not hold before the neutrinos are decoupled and therefore cannot be substituted here. This is also not the same as $\mathcal{L}$, as defined in eq. 33; $\mathcal{L}$ is the sum of L_{ν_α}s.

4. Density

From the number density, we can calculate the neutrino density.

$$\rho_{tot,\nu_\alpha} = \rho_{\nu_\alpha} + \rho_{\bar{\rho}_\alpha} \tag{A44}$$

$$\rho_{\nu_\alpha} = \frac{1}{2\pi^2} \int_0^\infty \frac{p_\nu E_\nu^2 dE_\nu}{e^{E_\nu/T - \eta} + 1} \tag{A45}$$

$$E_\nu \approx p \tag{A46}$$

$$\rho_{\nu_\alpha} = \frac{T_\nu^4}{2\pi^2} F_3(\eta_{\nu_\alpha}) \tag{A47}$$

$$\rho_{tot,\nu_\alpha} = \frac{T_\nu^4}{2\pi^2} \left(F_3(\eta_{\nu_\alpha}) + F_3(-\eta_{\nu_\alpha})\right) \tag{A48}$$

We apply eq. A21:

$$\rho_{tot,\nu_\alpha} = \frac{T_\nu^4}{2\pi^2} \left[2F_3(0) + 6F_1(0)\eta_{\nu_\alpha}^2 + \frac{1}{4}\eta_{\nu_\alpha}^4\right] \tag{A49}$$

$$\rho_{tot,\nu_\alpha} = \frac{14}{8}\frac{\pi^2}{30} T_\nu^4 \left[1 + \frac{30}{7\pi^2}\eta_{\nu_\alpha}^2 + \frac{15}{7\pi^4}\eta_{\nu_\alpha}^4\right] \tag{A50}$$

If η is 0, this reduces to the standard Fermi-Dirac distribution:

$$\rho_{FD} = \frac{7}{8} g \frac{\pi^2}{30} T^4 \tag{A51}$$

Appendix B: Data

1. Tables

The D/H ratio, ^{4}He mass fraction, and $\tilde{N}_{eff}$ are shown in table B 1.

2. Spectra

The full data set generated including energy spectra can be found at `lgilbert.co/thesis/data/thesisdata.zip`.

[1] C. Dib, J. C. Helo, S. Kovalenko, and I. Schmidt, Phys. Rev. D **84**, 071301 (2011), arXiv:1105.4664 [hep-ph].

[2] G. Mention, M. Fechner, T. Lasserre, T. A. Mueller, D. Lhuillier, M. Cribier, and A. Letourneau, Phys. Rev. D **83**, 073006 (2011), arXiv:1101.2755 [hep-ex].

[3] J. Kopp, P. A. N. Machado, M. Maltoni, and T. Schwetz, Journal of High Energy Physics **5**, 50 (2013), arXiv:1303.3011 [hep-ph].

[4] R. J. Cooke, M. Pettini, R. A. Jorgenson, M. T. Murphy, and C. C. Steidel, Astrophys. J. **781**, 31 (2014), arXiv:1308.3240.

[5] D. Tytler, D. Kirkman, C. Zeisse, D. Lubin, A. Day, J. Lee, and B. Ou, "QSO Light on New Physics," NOAO Proposal (2010).

[6] G. Mangano, G. Miele, S. Pastor, and M. Peloso, Physics Letters B **534**, 8 (2002), arXiv:astro-ph/0111408.

[7] Planck Collaboration, P. A. R. Ade, N. Aghanim, M. Arnaud, M. Ashdown, J. Aumont, C. Baccigalupi, A. J. Banday, R. B. Barreiro, J. G. Bartlett, and et al., ArXiv e-prints (2015), arXiv:1502.01589.

[8] C. T. Kishimoto and G. M. Fuller, Phys. Rev. D **78**, 023524 (2008), arXiv:0802.3377.

[9] C. T. Kishimoto, G. M. Fuller, and C. J. Smith, Physical Review Letters **97**, 141301 (2006), astro-ph/0607403.

[10] A. D. Dolgov, S. H. Hansen, S. Pastor, S. T. Petcov, G. G. Raffelt, and D. V. Semikoz, Nuclear Physics B **632**, 363 (2002), hep-ph/0201287.

[11] E. Grohs, G. M. Fuller, C. T. Kishimoto, and M. W. Paris, JCAP **5**, 017 (2015), arXiv:1502.02718.

[12] L. Kawano, (1992).

[13] G. M. Fuller and C. J. Smith, Phys. Rev. D **82**, 125017 (2010), arXiv:1009.0277 [astro-ph.CO].

[14] M. Pettini and R. Cooke, MNRAS **425**, 2477 (2012), arXiv:1205.3785.

[15] Y. I. Izotov, T. X. Thuan, and N. G. Guseva, MNRAS **445**, 778 (2014), arXiv:1408.6953.

[16] K. Abazajian, N. F. Bell, G. M. Fuller, and Y. Y. Y. Wong, Phys. Rev. D **72**, 063004 (2005), astro-ph/0410175.

[17] E. Grohs, G. M. Fuller, C. T. Kishimoto, and M. W. Paris, Phys. Rev. D **92**, 125027 (2015), arXiv:1412.6875.

[18] H. Mo, F. V. d. Bosch, and S. White, *Galaxy formation and evolution* (Cambridge University Press, 2010).

TABLE I. Data for 1 eV sterile neutrinos, 10 eV sterile neutrinos, and a three neutrino system.

	D/H	^{4}He	N_{eff}	$\tilde{N}_{eff}$
$m_s = 1$ eV, $\theta = 3^* 10^{-1}$, $\mathcal{L}_{\nu_\alpha} = 2 * 10^{-2}$	2.63460E-05	0.245170	3.00220	2.99330
$m_s = 1$ eV, $\theta = 3 * 10^{-2}$, $\mathcal{L}_{\nu_\alpha} = 2 * 10^{-2}$	2.64190E-05	0.246430	3.00220	2.99100
$m_s = 1$ eV, $\theta = 3 * 10^{-3}$, $\mathcal{L}_{\nu_\alpha} = 2 * 10^{-2}$	2.61810E-05	0.242320	3.00220	2.99930
$m_s = 1$ eV, $\theta = 3 * 10^{-4}$, $\mathcal{L}_{\nu_\alpha} = 2 * 10^{-2}$	2.61250E-05	0.241370	3.00190	3.00140
$m_s = 1$ eV, $\theta = 3 * 10^{-1}$, $\mathcal{L}_{\nu_\alpha} = 2 * 10^{-3}$	2.66270E-05	0.250030	3.00110	2.99520
$m_s = 1$ eV, $\theta = 3 * 10^{-2}$, $\mathcal{L}_{\nu_\alpha} = 2 * 10^{-3}$	2.65000E-05	0.247860	3.00110	2.99970
$m_s = 1$ eV, $\theta = 3 * 10^{-3}$, $\mathcal{L}_{\nu_\alpha} = 2 * 10^{-3}$	2.64630E-05	0.247240	3.00090	3.00090
$m_s = 1$ eV, $\theta = 3 * 10^{-4}$, $\mathcal{L}_{\nu_\alpha} = 2 * 10^{-3}$	2.64550E-05	0.247100	3.00110	3.00110
$m_s = 1$ eV, $\theta = 3 * 10^{-1}$, $\mathcal{L}_{\nu_\alpha} = 2 * 10^{-4}$	2.65020E-05	0.247900	3.00110	3.00090
$m_s = 1$ eV, $\theta = 3 * 10^{-2}$, $\mathcal{L}_{\nu_\alpha} = 2 * 10^{-4}$	2.64950E-05	0.247790	3.00100	3.00100
$m_s = 1$ eV, $\theta = 3 * 10^{-3}$, $\mathcal{L}_{\nu_\alpha} = 2 * 10^{-4}$	2.64910E-05	0.247720	3.00110	3.00110
$m_s = 1$ eV, $\theta = 3 * 10^{-4}$, $\mathcal{L}_{\nu_\alpha} = 2 * 10^{-4}$	2.64910E-05	0.247710	3.00110	3.00110
$m_s = 10$ eV, $\theta = 3 * 10^{-1}$, $\mathcal{L}_{\nu_\alpha} = 2 * 10^{-2}$	2.62700E-05	0.243870	3.00220	3.01980
$m_s = 10$ eV, $\theta = 3 * 10^{-2}$, $\mathcal{L}_{\nu_\alpha} = 2 * 10^{-2}$	code crashes	code crashes	code crashes	code crashes
$m_s = 10$ eV, $\theta = 3 * 10^{-3}$, $\mathcal{L}_{\nu_\alpha} = 2 * 10^{-2}$	2.61810E-05	0.242320	3.00220	2.99930
$m_s = 10$ eV, $\theta = 3 * 10^{-4}$, $\mathcal{L}_{\nu_\alpha} = 2 * 10^{-2}$	2.61220E-05	0.241280	3.00280	3.00740
$m_s = 10$ eV, $\theta = 3 * 10^{-1}$, $\mathcal{L}_{\nu_\alpha} = 2 * 10^{-3}$	2.65060E-05	0.247970	3.00110	3.00900
$m_s = 10$ eV, $\theta = 3 * 10^{-2}$, $\mathcal{L}_{\nu_\alpha} = 2 * 10^{-3}$	2.78380E-05	0.274440	2.90190	2.90410
$m_s = 10$ eV, $\theta = 3 * 10^{-3}$, $\mathcal{L}_{\nu_\alpha} = 2 * 10^{-3}$	2.64950E-05	0.247780	3.00110	2.90190
$m_s = 10$ eV, $\theta = 3 * 10^{-4}$, $\mathcal{L}_{\nu_\alpha} = 2 * 10^{-3}$	2.64560E-05	0.247110	3.00110	3.00160
$m_s = 10$ eV, $\theta = 3 * 10^{-1}$, $\mathcal{L}_{\nu_\alpha} = 2 * 10^{-4}$	2.64920E-05	0.247730	3.00110	3.00140
$m_s = 10$ eV, $\theta = 3 * 10^{-2}$, $\mathcal{L}_{\nu_\alpha} = 2 * 10^{-4}$	2.64920E-05	0.247740	3.00110	3.00150
$m_s = 10$ eV, $\theta = 3 * 10^{-3}$, $\mathcal{L}_{\nu_\alpha} = 2 * 10^{-4}$	2.64910E-05	0.247720	3.00110	3.00130
$m_s = 10$ eV, $\theta = 3 * 10^{-4}$, $\mathcal{L}_{\nu_\alpha} = 2 * 10^{-4}$	2.64910E-05	0.247710	3.00110	3.00110
three neutrinos, $\mathcal{L}_{\nu_\alpha} = 2 * 10^{-2}$	2.60990E-05	0.240890	3.00220	3.00220
three neutrinos, $\mathcal{L}_{\nu_\alpha} = 2 * 10^{-3}$	2.64540E-05	0.247090	3.00110	3.00110
three neutrinos, $\mathcal{L}_{\nu_\alpha} = 2 * 10^{-4}$	2.64910E-05	0.247710	3.00110	3.00110
three neutrinos, $\mathcal{L}_{\nu_\alpha} = 0$	2.64950E-05	0.247780	3.00110	3.00110